

# Comparison Between Analog and Digital Neural Network Implementations for Range-Finding Applications

Laurent Gatet, *Member, IEEE*, Hélène Tap-Béteille, *Member, IEEE*, and Francis Bony

**Abstract**—A neural network (NN) was developed in order to increase the distance range of a phase-shift laser range finder and to achieve surface recognition, by using two photoelectrical signals issued from the measurement system. The NN architecture consists of a multilayer perceptron (MLP) with two inputs, three neurons in the hidden layer, and one output. Depending on the application, the NN output has to resolve the ambiguity due to phase-shift measurement by linearizing the inverse of the square law, or to indicate an output voltage corresponding to the tested surface. This embedded system dedicated to optoelectronic measurements was successfully tested with an analog NN, implemented in  $0.35\text{-}\mu\text{m}$  complimentary metal-oxide-semiconductor (CMOS) technology, resulting in a threefold increase in the distance range with respect to the one limited by the phase-shift measurement, and by discriminating four types of surfaces (a plastic surface, glossy paper, a painted wall, and a porous surface), at a remote distance between the range finder and the target varying from 0.5 m up to 1.25 m and with a laser beam angle varying between  $-\pi/6$  and  $\pi/6$  with respect to the target. In this type of application, NN analog implementation provides many advantages, notably use of a small silicon area, low power consumption and no analog-to-digital conversions (ADCs). Nevertheless, digital implementation allows ease of conception and reconfigurability and an embedded weight and bias update. This paper presents the complete measurement system and a comparison between both types of implementation, by developing the advantages and drawbacks relative to each method. An optimized mixed architecture, using both techniques, is then proposed and discussed at the end of the paper.

**Index Terms**—Analog and digital neural network implementations, distance range increase, laser range finder, multilayer perceptron, surface classification.

Manuscript received November 08, 2007; revised June 05, 2008 and June 05, 2008; accepted October 31, 2008. First published January 27, 2009; current version published February 27, 2009.

L. Gatet was with the Laboratory of Optoelectronics for Embedded Systems (LOSE), Electronics, Electrotechnology, Computer Science, Hydraulics, and Telecommunications Engineering School (ENSEEIHT), National Polytechnic Institute (INP), Université de Toulouse, F-31071, Toulouse Cedex 7, France. He is now with the National Center of Spatial Studies (CNES), Toulouse F-31401, France (e-mail: gatet@enseeiht.fr).

H. Tap-Béteille and F. Bony are with the Laboratory of Optoelectronics for Embedded Systems (LOSE), Electronics, Electrotechnology, Computer Science, Hydraulics, and Telecommunications Engineering School (ENSEEIHT), National Polytechnic Institute (INP), Université de Toulouse, F-31071, Toulouse Cedex 7, France (e-mail: beteille@enseeiht.fr; bony@enseeiht.fr).

Color versions of one or more of the figures in this paper are available online at <http://ieeexplore.ieee.org>.

Digital Object Identifier 10.1109/TNN.2008.2009120

## I. INTRODUCTION

INSTANCE measurement [1], surface classification [2]–[4], object detection [5], [6], and pattern recognition [7]–[10] are determinant in many fields, such as assistance and obstacle detection for autonomous robots or vehicles [11]–[14], identification, surveillance, and security systems [15]–[18], medical applications [19], industrial processes [20], [21], and navigation [18], [22], [23]. Depending on the type of application, different types of sensors may be used to measure distance and/or to detect surfaces: optical (in visible [14], [24], in infrared [11], [22], [25], or in multispectral wavelengths [17]), ultrasonic [1], [26], radar-, sonar-, or lidar-based [3], [5], [18], and so on. The optical techniques of instrumentation using laser beams are often limited in resolution and/or in distance range, due to optic saturation, noise, and measurement conditions. Moreover, there is no system nor procedure capable of discriminating a wide range of surface types. Furthermore, target detection systems are often limited by the fact that distance and/or incidence angle between the sensor and the target have to be set.

The aim of this work is to realize a complete real-time measurement system which could be implemented in various applications such as distance control or pieces quality control in industry, distance evaluation of obstacles in robotics, road surface inspection, space applications, and so on. The optoelectronic system chosen for achieving high-resolution measurements is a phase-shift laser range finder, using a single high-frequency modulated laser diode [27]. The aim of this project is to implement a system capable of increasing the measurement range of the range finder limited by the phase-shift measurement, and to allow surface discrimination on a wide distance range, just by using signals already present in the range-finding system, without changing its structure or adding another measurement system or achieving complex data processing. The power consumption of the added structure and its size have to be optimized in order to be embedded directly in the optical head of the range finder. Finally, this system must be reconfigurable as a function of the experimental conditions.

One way to improve distance measurement and to achieve surface discrimination is to use artificial neural networks (NNs) [1]–[11], [16]–[18], [21], [23]–[26]. Multilayer perceptrons (MLP) are notably used to approximate nonlinear functions continuously, in order to linearize distorted transfer characteristics or to achieve classification on extended ranges due to limited experimental data values [2], [3], [24], [28]. Two

feasibility studies have previously been developed: the first one in order to resolve the  $2k\pi$ -ambiguity of a phase-shift laser range finder, and the second one to achieve surface detection on wide distance ranges, using a neural network [29]. By combining both well-known techniques of distance measurement and signal processing, it is possible to triple the measurement range without changing the resolution or the structure of the range finder, and to recognize different types of surfaces in a distance range of around 1 m with a varying angle between the phase-shift laser range finder and the target [29].

As behavioral simulations had shown satisfying results, the neural network was designed and then implemented with analog circuits to avoid analog-to-digital conversions (ADCs) [30], [31]. After having determined the complete transfer characteristic of the analog feedforward MLP-type NN with respect to its inputs and its parameters, it has been validated with experimental data issued from the range-finding system. The complete optoelectronic measurement system structure and the experimental results relative to both applications are presented in Sections II and III.

The overall system was validated under well-defined experimental conditions. The next development step is the adaptation of the NN parameters, so that the sensor achieves its task autonomously, whatever the experimental conditions. Thus, it is necessary to implement the parameters' updating system directly on-chip. If the updating system is digital, as is common, the number of ADCs and DACs will depend on the number of NN parameters and analog data issued from the range finder. This is why a discussion has to be held in Section IV on the type of NN implementation in order to select the right choices for optimizing the main criteria associated with embedded systems, i.e., high precision, low power consumption, low cost, conception easiness, reconfigurability, and simplicity. The elementary analog MLP-type implemented NN is compared with a digital one, in order to determine the advantages and the drawbacks relative to each method. An optimized NN mixed architecture, using both techniques, is proposed and discussed at the end of this paper.

## II. OPERATING PRINCIPLE

The sensor operating principle is presented in Fig. 1. The phase-shift laser range finder [27] is located at a distance  $D$  of a Lambertian target, with an observation angle  $\theta_0$ . The distance  $D$  between the sensor and the target is deduced by evaluating the phase-shift  $\Delta\varphi$  between the emitted and received signals, proportional to the time of flight  $\tau_D$ . A heterodyne technique is used in order to measure the phase shift at a lower intermediate frequency. The range-finder output signal  $VoutRANG$ , proportional to the phase-shift measurement  $\Delta\varphi$ , can be written as

$$\begin{aligned} VoutRANG &= K \cdot \Delta\varphi = K \cdot 2\pi f_{RF} \tau_D = K \cdot 2\pi f_{RF} \frac{2D}{c} \\ &= K_2 D \end{aligned} \quad (1)$$

with  $K$  being the proportionality coefficient between phase-shift and range-finder output signal,  $f_{RF}$  being the modulation frequency,  $c$  being the light speed, and  $K_2$  being the proportionality coefficient between distance and range-finder output signal.

### A. Measurement Range Increase

As phase shift is measured modulo  $2\pi$ , distance value is given with a “ $2k\pi$ -ambiguity.” The maximum measurement range  $\Lambda$  without ambiguity is

$$\Lambda = \frac{c}{2f_{RF}}. \quad (2)$$

Thus, for high modulation frequencies  $f_{RF}$ , the high precision obtained on distance measurement is limited to a small distance range.

In order to resolve the  $2k\pi$ -ambiguity, the most common solution is to modulate the laser diode with two frequencies, a high frequency to have a high resolution on measurement and a lower one to increase the distance range [32]. However, the heterodyne technique is complex to apply with this method. Furthermore, as the aim is to increase the distance range without making the range-finding structure more complex, the idea is to extract an approximation of the distance from another signal varying with distance and which is not limited by the  $2k\pi$  limitation. The filtered photoelectric signal amplitude  $VoutBP$ , measured at the bandpass filter output, depends on the distance  $D$  as follows [33]:

$$VoutBP = K_1 \frac{\rho \cos(\theta_0)}{D^2} \quad (3)$$

with  $K_1$  being a constant relative to the emitter, the optical transfer, and the response of the avalanche photo diode (APD), and  $\rho$  being the noncooperative target diffusing reflection coefficient. Thus, by using an MLP-type NN for approximating continuously the inverse of the root square function and linearizing its output with respect to the distance, it is possible to evaluate, approximately, the value of the distance in order to resolve the  $2k\pi$ -ambiguity due to phase-shift measurement.

It is admitted that the resolution of the distance measurement given at the NN output will be no better than the one obtained at the range-finder output, even if it is constituted by many hidden neurons. However, NN distance measurement range will be higher because it is only limited by input voltage dynamic and noise. In this application, NN role is not to perform a precise measurement but to evaluate “roughly” the distance in order to resolve the  $2k\pi$ -ambiguity caused by the phase-shift measurement.

### B. Surface Discrimination

The filtered photoelectric signal amplitude  $VoutBP$ , measured at the bandpass filter output, depends on the type of the surface tested through the noncooperative target diffusing reflection coefficient  $\rho$ . Thus, it is possible to achieve surface discrimination by extracting coefficient  $\rho$  from (3), however, as voltage  $VoutBP$  depends also on the distance  $D$  and the angle  $\theta_0$ , classification may not be achieved at large intervals.

In order to increase the measurement range, the proposed solution is to use the range-finder output signal  $VoutRANG$  (1), proportional to the distance. By using both signals, it is possible to achieve surface detection in a certain range of distance and angle  $\theta_0$  using a two-inputs MLP-type NN as a classifier (Fig. 1) [29]. The NN has to be calibrated so that its output corresponds to the tested target. Each type of surface is linked with

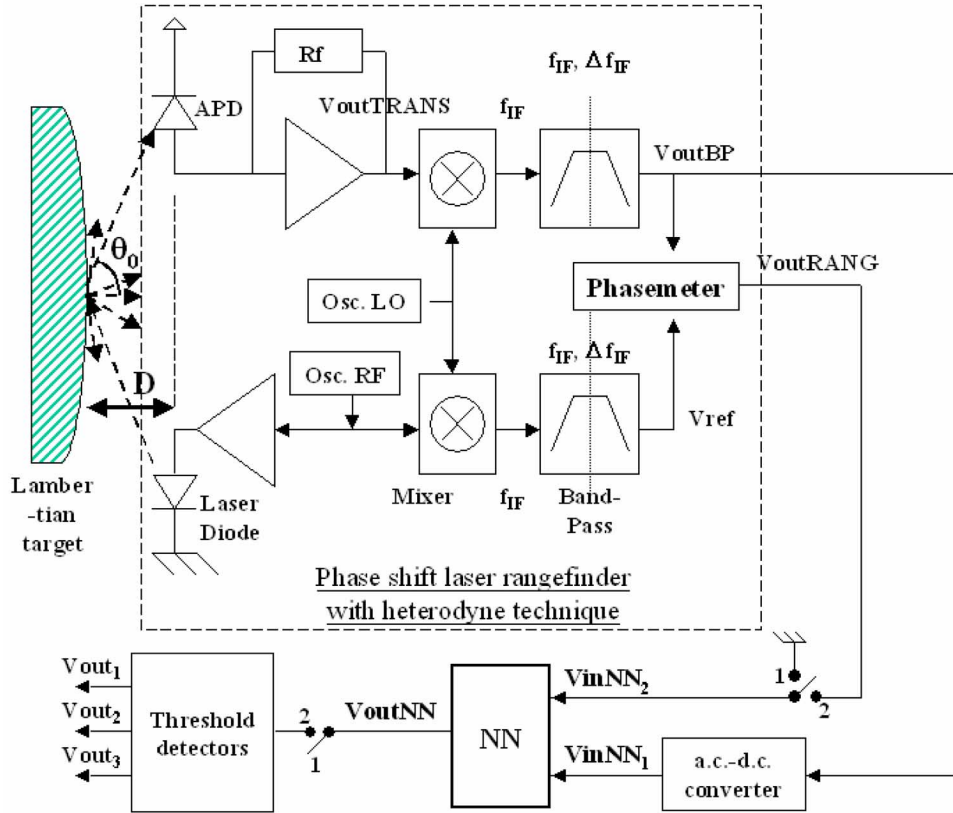


Fig. 1. Block diagram of the complete sensor system, constituted by the phase-shift laser range finder using a heterodyne technique and the NN followed by threshold comparators. Bandpass filters tuned to the intermediate frequency enhance the signal-to-noise ratio (SNR) of the photoelectric signal.

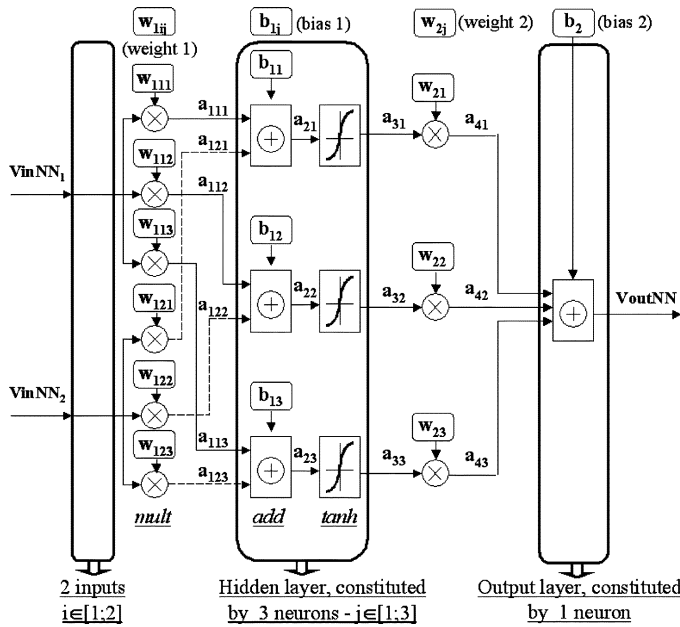


Fig. 2. Neural network architecture.

a specific output voltage range. Three threshold detectors have been placed at the NN output in order to easily show the interval to which the NN output voltage belongs [29].

### C. Overall Embedded System Dedicated to Optoelectronic Measurement

Depending on the application, the chosen switches represented in Fig. 1 are placed in position “1” or “2.” If the system is used to measure distances with high resolution on wide distance ranges, switches are set in position “1,” because in this case, the NN only needs to extract the distance value from the signal VoutBP, not limited by the  $2k\pi$ -ambiguity. If the system is selected to perform surface discrimination, switches are set in position “2,” in order to use both signals issued from the range finder and to perform thresholds detection at the NN output. In order to simplify the system, alternating current (ac) signal VoutBP is converted into a direct current (dc) voltage VinNN<sub>1</sub>, proportional to the root mean square (RMS) of VoutBP (Fig. 1).

Thus, with this system, it is possible to increase the range-finder measurement range limited by the phase-shift measurement, and to allow surface discrimination, just by using signals belonging to the range-finding system, without modifying its structure or needing any additional measurement systems nor achieving any complex data processing. Furthermore, as the NN transfer characteristic depends on its parameters, the system can be reconfigured depending on the experimental conditions. Finally, it is possible to implement the MLP-type NN structure in order for it to be directly embedded in the optical head of the range finder and to achieve its task onboard the system.

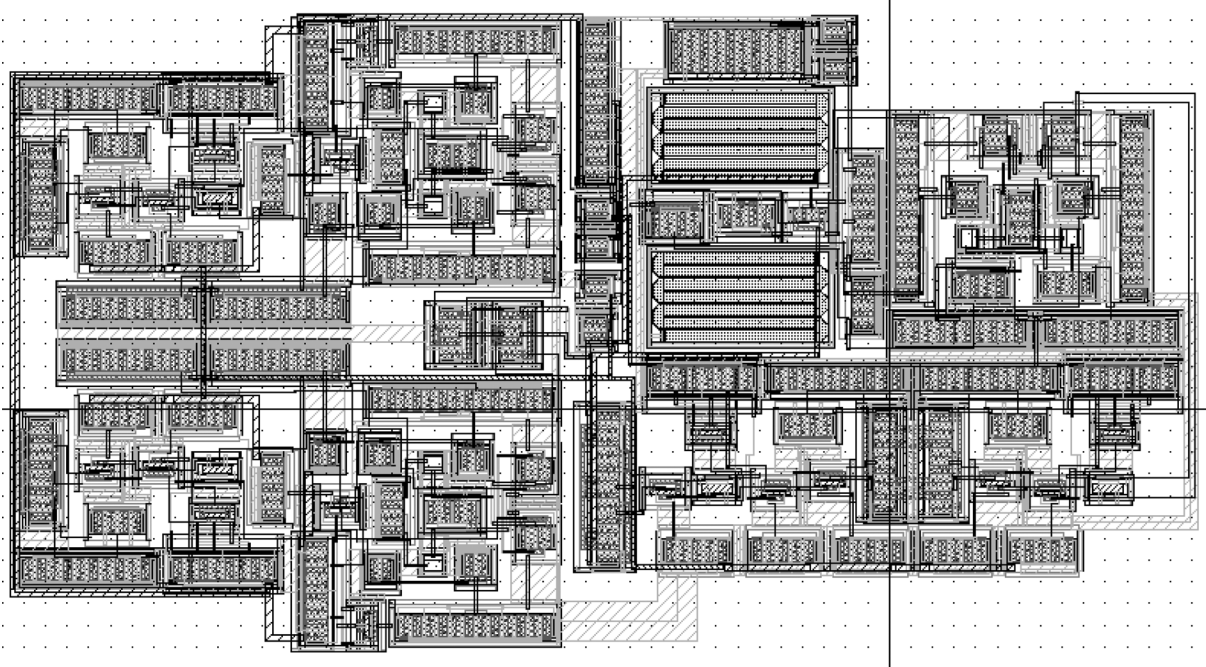


Fig. 3. Neuron layout with AMS CMOS  $0.35\text{ }\mu\text{m}$ . Size:  $276\text{ }\mu\text{m} \times 148\text{ }\mu\text{m}$ .

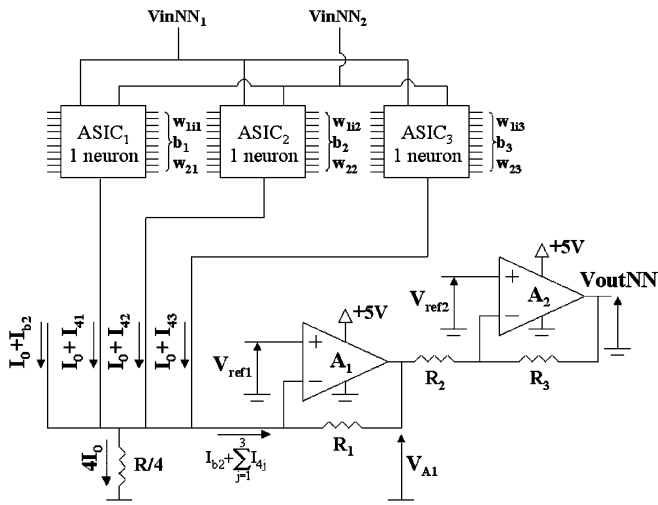


Fig. 4. Output layer schematic.

### III. ANALOG NEURAL NETWORK CONCEPTION

#### A. Analog NN Structure, Design, and Implementation

As mentioned previously, the chosen NN structure is an MLP-type in order to approximate functions continuously. Its architecture is represented in Fig. 2. It is composed of two input neurons, corresponding to both signals issued from the range finder. The input voltages VinNN<sub>1</sub> and VinNN<sub>2</sub> are, respectively, proportional to VoutBP and VoutRANG. The number of neurons in the output layer is equal to one. It provides a voltage VoutNN, which is proportional to the distance if switches are placed in position “1,” or which belongs to the interval dedicated to the tested surface if switches are placed in position “2.” The NN is constituted by a single hidden layer with three processing

neurons, whose activation function is a sigmoid (tanh). Behavioral simulations have shown that this number of hidden neurons is sufficient in order to increase the measurement range with a factor of three and to achieve surface discrimination without error on a distance range close to 1 m [29].

Then, it was decided to implement the MLP-type NN structure in order for it to be directly embedded in the optical head of the range finder and to achieve its task onboard the system. An elementary part of the NN, called neuron, was designed, laid out, and implemented with analog cells in order to avoid ADCs [30], [31]. One of the benefits of integrating the analog NN in an ASIC is the reduction of the circuits size. The chosen complimentary metal–oxide–semiconductor (CMOS)  $0.35\text{-}\mu\text{m}$  technology allows sufficient bandwidth and supply voltage in order to optimize the speed, the overall circuits consumption, and the signal dynamics. Each cell has been optimized in terms of linearity, in order to improve the voltage range for each input and each parameter. The layout of the elementary neuron is represented in Fig. 3. Nineteen pins of the JLCC44 ASIC are used for the neuron: three pins for grounds and supply voltage, six pins for VinNN<sub>1</sub>, VinNN<sub>2</sub>, w<sub>11j</sub>, w<sub>12j</sub>, b<sub>1j</sub>, and w<sub>2j</sub>, two pins for biasing the neuron and the hyperbolic tangent cell currents, and eight test pins placed at the main cells output buffer.

The complete NN was implemented on a printed circuit board (PCB) with three integrated neurons in parallel [31]. The output neuron was achieved with discrete components (Figs. 4 and 5). Measurements showed that the most fitting dc transfer function of the complete NN is [31]

$$\begin{aligned} \text{VoutNN} = & 2,5 + 6,75 \cdot b_2 + \frac{R_1}{R} \frac{R_3}{R_2} \sum_{j=1}^3 \cdot 1,17 \cdot w_{2j} \\ & \cdot \tanh(8 \cdot (2,3 \cdot w_{11j} \text{VinNN}_1 + 2,3 \\ & \cdot w_{12j} \text{VinNN}_2 + 0,6 \cdot b_{1j})) \end{aligned} \quad (4)$$

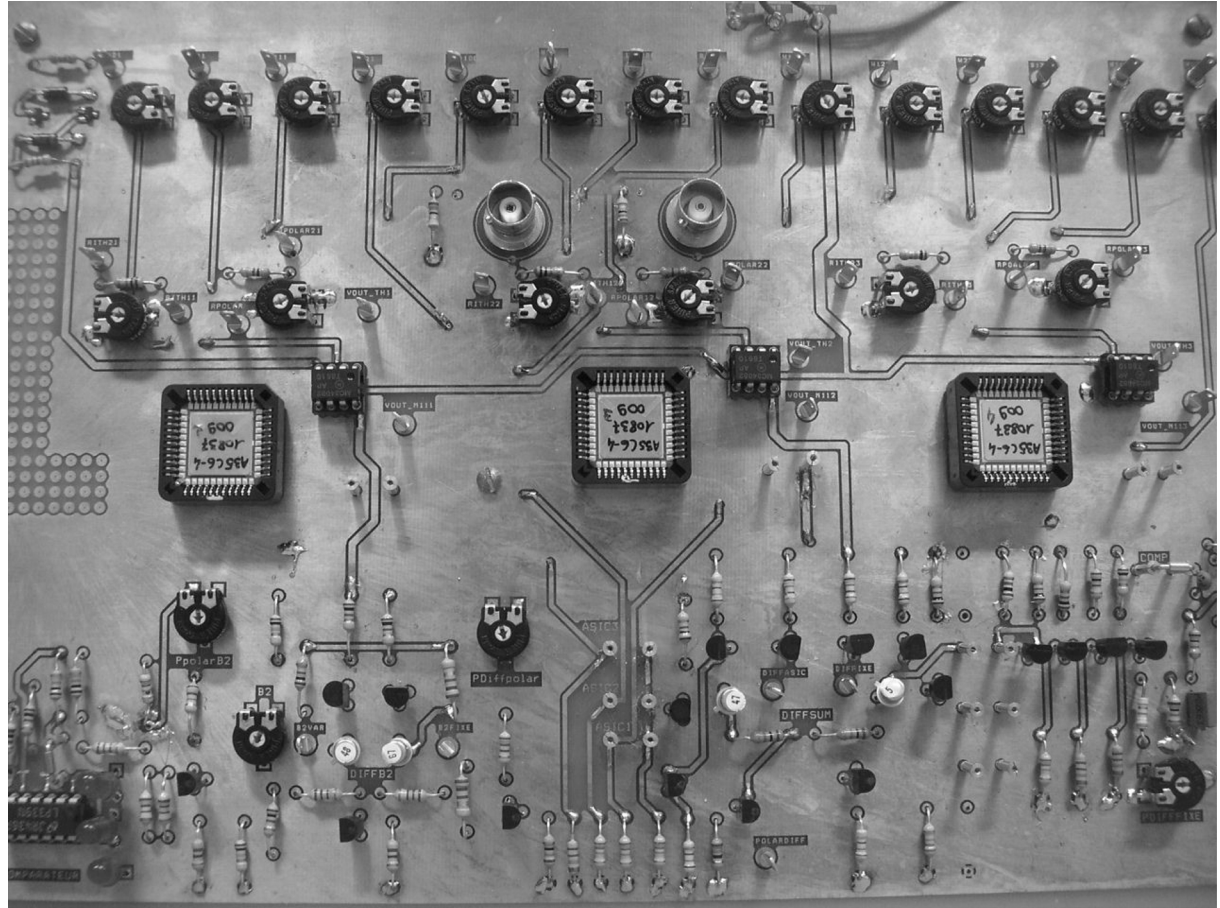


Fig. 5. Representation of the complete ANN on PCB, with one neuron implemented in each ASIC and the output neuron directly implemented on the PCB.

As it is difficult to quantify the error in terms of percentage, due to the high number of parameters involved, absolute error values between each test point and the corresponding value calculated with (4) have been summed together, in order to determine the mean error value  $e_{\text{mean}}$ . The mean error illustrates that the NN output value after training the NN using a simulation software will be measured at the implemented NN output with a mean precision  $e_{\text{mean}}$ . NN mean error  $e_{\text{mean}}$  with regards to (4) is equal to 30 mV, for any value of  $V_{\text{inNN}_1}$  or  $V_{\text{inNN}_2}$  or weight voltages  $w_{11j}, w_{12j}$  or  $w_{2j}$  belonging to the range of  $[-0.5 \text{ V}; 0.5 \text{ V}]$ , or bias voltages  $b_{1j}$  belonging to the range of  $[-0.15 \text{ V}; 0.15 \text{ V}]$ , or  $b_2$  belonging to the range of  $[-60 \text{ mV}; 60 \text{ mV}]$ . Error values above  $e_{\text{mean}}$  are obtained for input, weight, and bias values never used in practical cases.

Each ASIC neuron and PCB output neuron current consumptions are, respectively, equal to 4.25 and 2.25 mA (respectively, 4.35 and 2.15 mA in simulation). Thus, overall consumption of both simulated and tested NN is equal to 15 mA, which is sufficiently low in order for it to be directly embedded in the optical head of the range finder.

## *B. Experimental Tests Achieved on the Overall Embedded System Dedicated to Optoelectronic Measurement*

The NN training phase has been achieved with a software program in which the most fitting experimental transfer function (4) has been included. Thus, once the software training is finished,

software weight and bias values can be directly set on the PCB in order to verify the accurate approximation ability of the implemented NN.

**1) Measurement Range Increase:** Fig. 6(a) represents the dc voltage  $V_{inNN_1}$  proportional to the experimental voltage  $V_{outBP}$  provided by the range finder (Fig. 7). The nine represented dots correspond to the NN training values. Fig. 6(b) shows a comparison between the expected output voltage as a function of the distance (dashed curve), the simulated NN output voltage (solid curve), and the experimental NN output voltage (dotted curve). Fig. 6(c) represents the difference between simulated and experimental NN output voltages. The error between both curves is less than 30 mV, which was our design goal. Fig. 6(d) represents both simulated and experimental errors with respect to ideality—i.e., linear output voltage. Experimental error does not cross both dashed curves corresponding to the maximum error value; thus the analog NN is capable of approximating the inverse of the root square function in the whole distance range [0.5 m; 3.2 m] with sufficient precision so that the combination of this measurement with the one issued from the range-finder phase shift (limited to a distance range of 0.9 m) gives a high-resolution distance value on a distance range no longer limited by the  $2k\pi$ -ambiguity.

2) *Surface Discrimination*: An example of a test of a glossy paper target is presented in Fig. 8. Voltages  $V_{inNN_1}$  and  $V_{inNN_2}$  are set at both NN inputs for each tested surface, in the

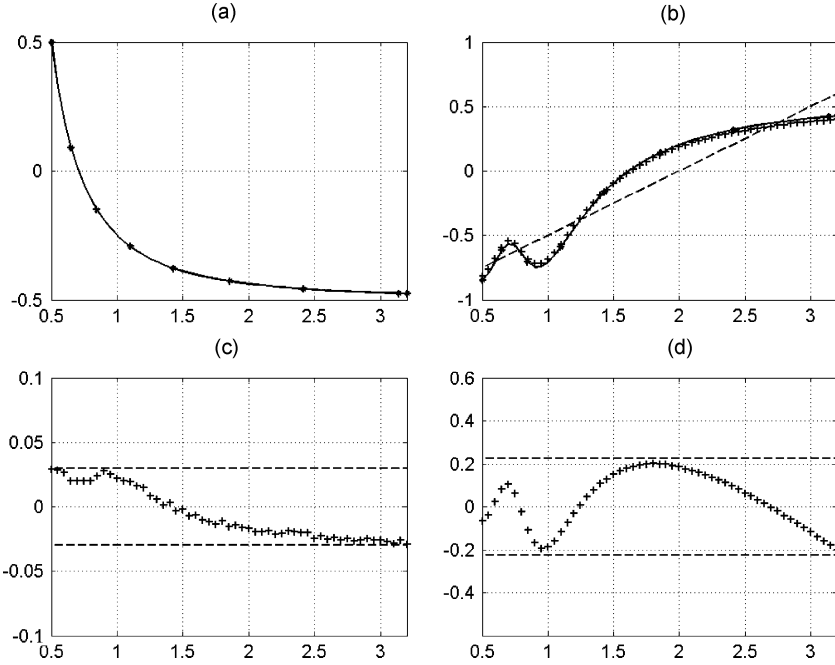


Fig. 6. Comparison between experimental tests, simulation, and ideality for a distance  $D$  varying between 0.5 and 3.2 m.

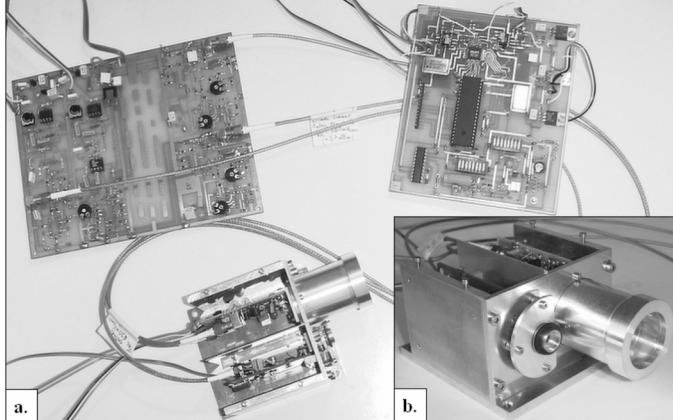


Fig. 7. (a) Photograph of a range finder. (b) Photograph of an optical head.

distance range [0.5 m; 1.25 m], for various angles  $\theta_0$  belonging to range  $[-\pi/6; \pi/6]$  [Fig. 8(a) and (b)]. In Fig. 8(c), the ideal output  $V_{outNNid} = 2.7$  V (bold dashed), the simulation results for nine angles  $\theta_0$  between  $-\pi/6$  and  $\pi/6$  (solid curve), and the corresponding experimental NN output voltage for angles  $\theta_0$  equal to 0 and  $\pm\pi/6$  (crosses) are represented. Fig. 8(d) shows the error between the simulation and the experimental tests. Dashed lines represent the mean error value  $\pm 30$  mV between the NN experimental tests and (4). It can be noticed that most of the points are located between both dashed curves. Absolute error value between the ideal output voltage  $V_{outNNid} = 2.7$  V and the experimental measurements is represented in Fig. 8(e). The dashed curve is relative to the maximum error value  $e_{max} = 0.2$  V that must not be reached in order to achieve a good detection of the considered surface by the threshold detectors. As each test point relative to angles 0 and  $\pm\pi/6$  is under the error limit voltage, the binary error indicated in

Fig. 8(f) is equal to 0 for each angle  $\theta_0$ , which means that the glossy paper is well discriminated from the other surfaces for every angle  $\theta_0$  from  $-\pi/6$  to  $\pi/6$ , in the distance range [0.5 m; 1.25 m]. The other figures corresponding to the three other types of tested surfaces were similar, and presented a binary error equal to 0 for each angle  $\theta_0$ , in the distance range [0.5 m; 1.25 m] [34].

#### IV. DIGITAL VERSUS ANALOG NEURON IMPLEMENTATION

The complete optoelectronic system containing the analog NN was validated under well-defined experimental conditions. The next development step, in order to make the system more autonomous and able to achieve distance evaluation and surface discrimination on wider ranges, is the design of the same architecture with a digital output feedback on weights and biases. Then, the sensor will be able to achieve its task in various test conditions (temperature, defocalization, crosstalk, and so on) and to allow NN onboard training in order to avoid computer calibration. The number of digital inputs/outputs needed to update each parameter is not high. Furthermore, the NN parameters update, which depends on the experimental conditions, need not be fast.

Nevertheless, if the system chosen in order to update the parameters of the analog NN is digital, the number of ADCs and DACs will depend on the number of NN parameters and analog data issued from the range finder [Fig. 9(a)]. The higher is the number of conversions, the higher will be the overall consumption and the system complexity.

Thereby, one could think that a digital NN could be more appropriate than an analog one since it limits the number of conversions [Fig. 9(b)]. That is the reason why one neuron was designed digitally in order to emphasize the advantages and the drawbacks of both analog and digital implementation methods.

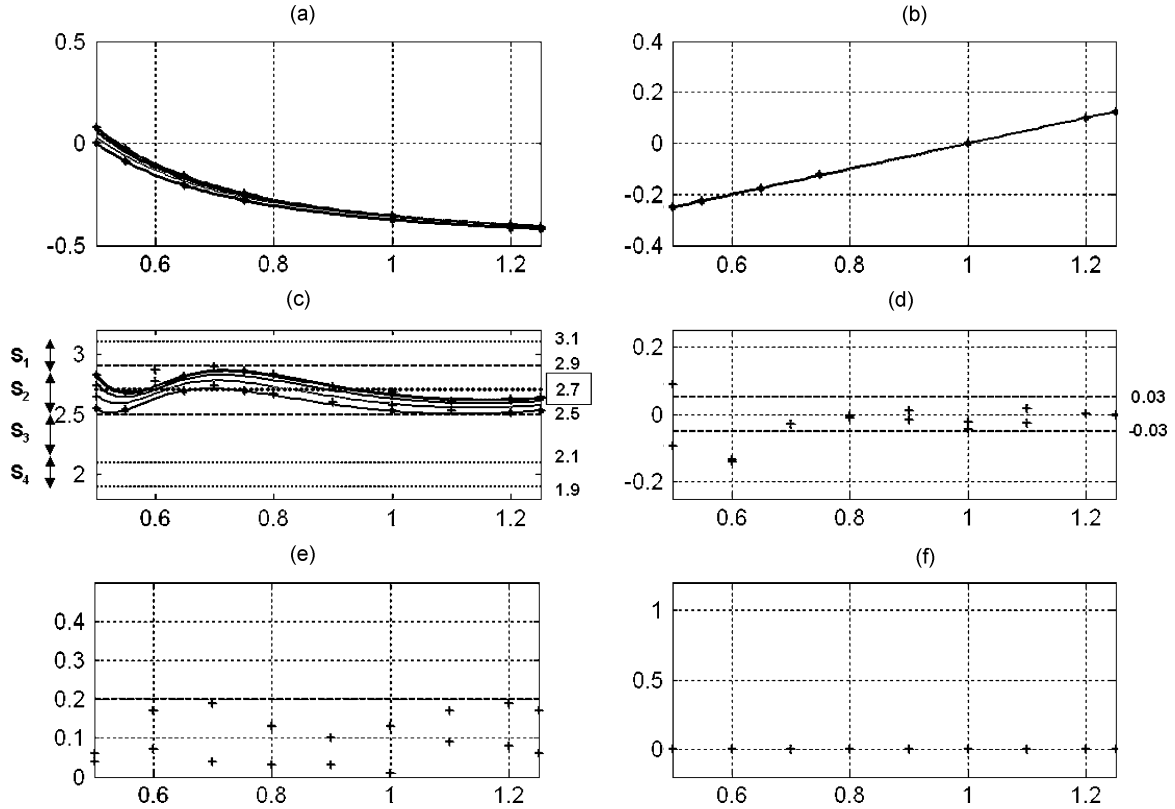


Fig. 8. Representation of the test results relative to the glossy paper for a distance  $D$  varying between 0.5 and 1.25 m.

#### A. Digital NN Structure

The center part of the digital neuron is the conception of the sigmoid activation function. Using a microprocessor or a digital signal processor (DSP) to synthesize it with a floating point coding will improve the precision. This solution will, however, increase the power consumption and the delay. Moreover, a software solution requires memory cells and sequential machine to stock and compute the program. The consequence is a larger occupied area in case of an implementation in an ASIC or a higher percentage of mobilization in case of a use of a field-programmable gate array (FPGA). For this, a hardware implementation was chosen instead of a software one, with fixed-point coding for the real number. The digital neuron was synthesized in an Xilinx Spartan 3 FPGA (XC3S200). The choice of this device was motivated by the presence of hardware signed multipliers.

In order to allow a comparison with the analog structure, the dynamics associated with each digital input and each parameter of the neuron was fixed to 1 V peak to peak. The precision has been defined to 1 mV, relative to the analog noise threshold. This leads to the coding of each parameter in 10 b and to the implementation of a 10-b ADC at each neuron input. The components synthesis was achieved in VHDL [VHSIC (very high-speed integrated circuits) hardware description language], with asynchronous operations in order to control the overall delay. Each multiplier and adder, whose output has been coded in 16 b, occupies, respectively, 50 and 8 slices, respectively distributed in 93 and 16 lookup tables (LUT).

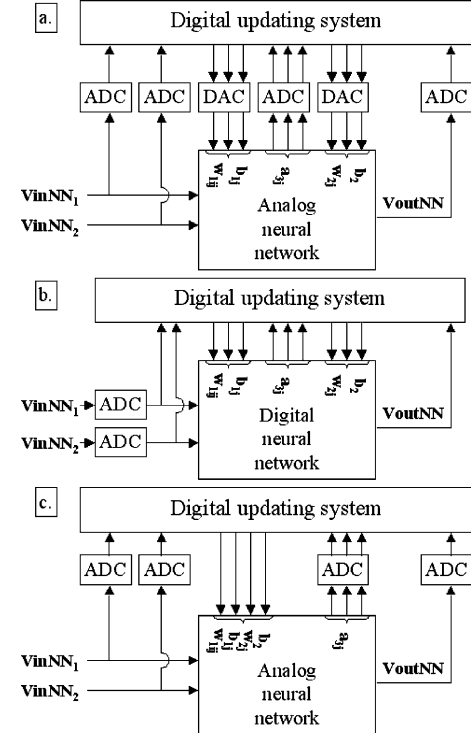


Fig. 9. (a) Analog neural network with digital updating system. (b) Digital neural network with digital updating system. (c) “Mixed-mode” neural network with analog current multipliers and current adders controlled by digital values.

Several methods exist to implement the sigmoid activation function, such as the Cordic algorithm usually used. Neverthe-

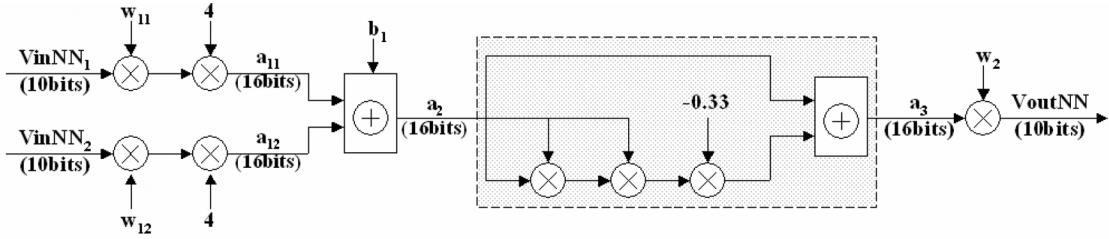


Fig. 10. Digital implementation schematic of the elementary neuron (104 slices distributed in 204 LUTs). The outlined part represents the sigmoid activation function limited to order three.

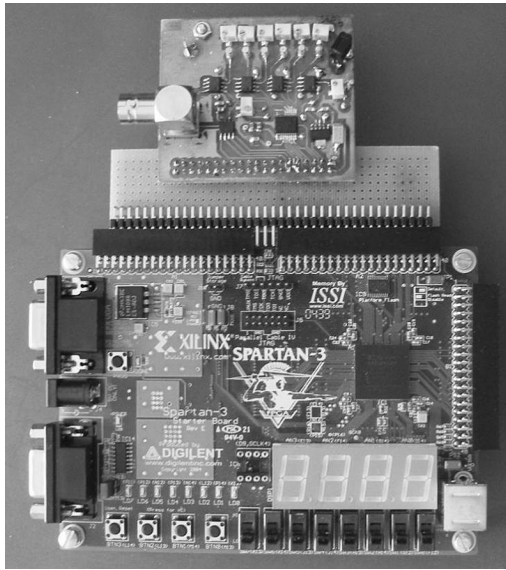


Fig. 11. Photograph of the PCB (on top) and the FPGA used for testing the digital elementary neuron.

less, the chosen method is the expanded Taylor's series with a limited order. It avoids the use of sequential circuits present in the Cordic method and enables optimization of the overall power consumption and the propagation delays. Furthermore, as the contribution of the terms whose order is superior to three is negligible in the 1-V domain, the development of the sigmoid was limited to order three. Thus, the neuron was implemented only with multipliers and adders, where Fig. 10 represents how they have been connected.

After postrouting simulations were validated, the neuron was implemented in the FPGA and then tested (Fig. 11). The transfer characteristic of each cell is very close to ideality (Fig. 12). For an input dynamic range of 1-V peak to peak, the multiplier output voltage was evaluated with a precision of 1 mV. The difference observed between ideal and real transfer characteristics of the sigmoid activation function is due to the expanded Taylor's series limited to order three. An approximation with a higher order development could give a characteristic closer to ideality, but with a higher overall consumption and a higher number of slices. The power consumption of the elementary neuron is equal to 37.2 mW, essentially due to the static random access memory (SRAM) consumption of the chosen FPGA.

### B. Comparison Between Both Implementations of the Elementary Neuron

Analog and digital implementations were compared respecting several criteria, such as power dissipation, occupied silicon area, design time, design cost, validation time, robustness to distortion, ease of use, and so on. Most of them, as listed in Table I, showed a lower power consumption and a faster signal propagation speed in the case of the analog neuron, for a comparable resolution. This confirms the first implementation choice in order to embed the feedforward network directly onboard the range finder.

Nevertheless, the design and the realization times are consequently larger. Concerning the design cost, the analog one is clearly more expensive than the digital one. Moreover, once the ASIC has been built, it is not possible to modify the implemented circuits, while the digital neural structure may always be reconfigured.

The validation time was almost identical for both implementations. In terms of ease of testing, the analog structure needs the offset measurement of each parameter due to transistor mismatches inside the ASIC. Concerning the digital neuron, an offset also appears at each digital-to-analog converter (DAC) output. Moreover, fixed-point coding involves truncation errors if the number of bits chosen for coding the decimal part is not sufficient. In our case, this error has been reduced by dedicating one bit for the sign, two bits for the integer part, and the rest of the code for the decimal part. By comparing both testing methods, calibrating the digital neuron was more complex due to the need to take into account each conversion between the analog and digital parts. For the analog neuron, once each offset has been determined, the plot of each cell transfer function was fast, and there was no difficulty in translating into analog values the parameters found after training the NN using a hardware simulation program.

Furthermore, by comparing both analog and digital cell characteristics, the analog multiplier is more sensitive to distortion. On the other hand, the digital hyperbolic tangent cell less than approaches the desired nonlinear function; however, a solution to optimize this function might be the use of a LUT. It might allow to reduce the number of arithmetic components and the propagation delay. If this LUT were introduced instead of the actual expanded Taylor's series limited to order three, the required memory size would be about 1 Mb. The use of another FPGA that might embed a larger memory would be necessary for testing this solution.

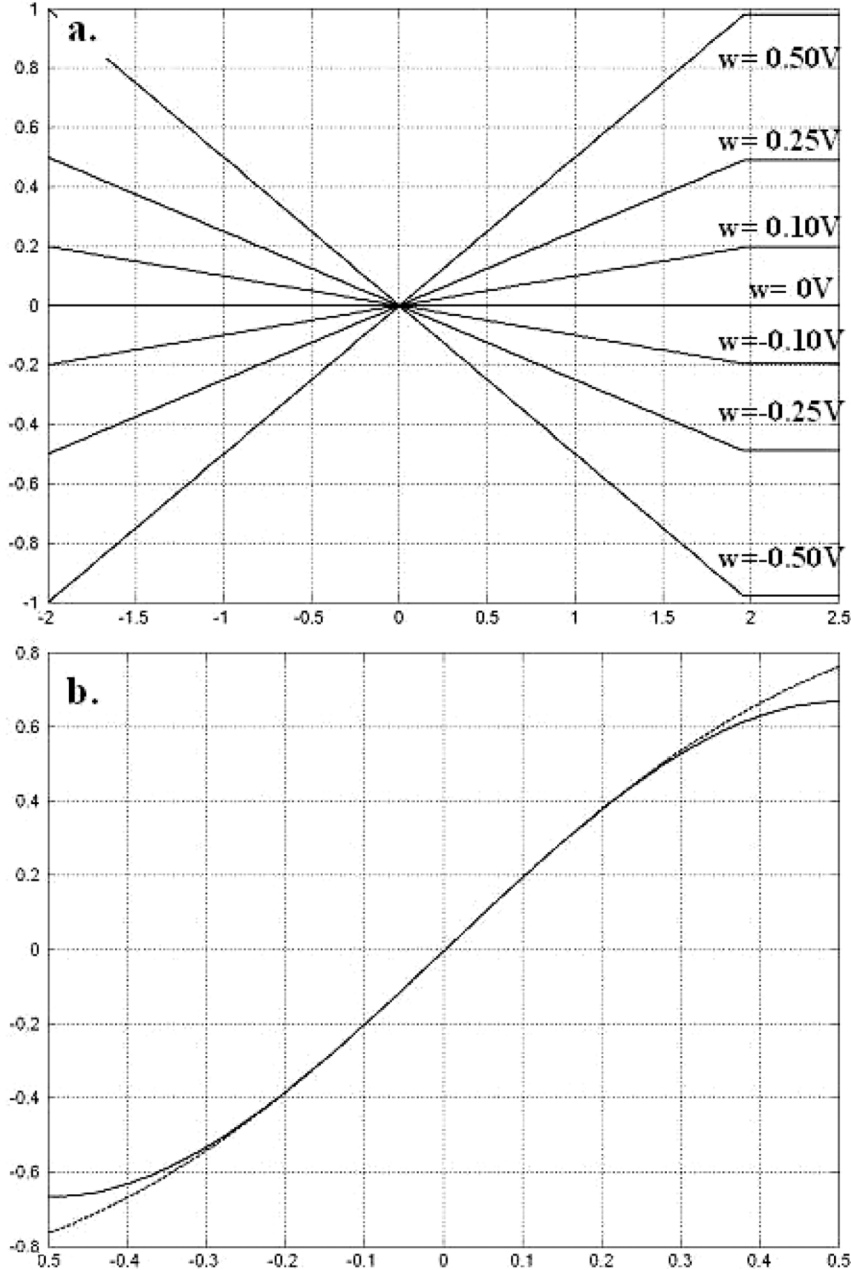


Fig. 12. (a) Output voltage (V) of one digital multiplier as a function of its input voltage (V), for weight values  $w$  varying between  $-0.5$  V and  $0.5$  V. Saturation appears for input values close to  $2$  V. (b) Output voltage (V) of one digital hyperbolic tangent cell (solid curve) as a function of its input voltage (V). The dashed curve represents the unabridged hyperbolic tangent, not limited to order three. The depicted values do not belong to “tanh” but to a scaled version.

Finally, in order to have a more rigorous comparison, it would be necessary to design the digital circuit in an ASIC. In this case, the complexity, the design time, and the cost are identical for both types of implementation, and the digital one loses its ability to be reconfigurable. Moreover, if we look at the transistor level, even if the sizes of the transistors involved in the digital implemented circuits are smaller, the number of mobilized transistors differs for a function of the cell and its required precision. For example, for the activation function, a single analog differential pair composed of two transistors is sufficient, while the number of digital transistors depends on the approximation order chosen for approximating the sigmoid characteristic. In this case, for an

equivalent precision, the area occupied by the digital implementation and the associated power consumption can be assumed to be larger than the analog one.

## V. CONCLUSION

The system presented in this paper easily allows the removal of the  $2k\pi$ -ambiguity on the phase-shift measurement and thus to obtain a measurement range three times wider, and to discriminate four types of surfaces (plastic surface, glossy paper, painted wall, and porous surface) for distances and angles, respectively, varying between [0.5 m; 1.25 m] and  $[-\pi/6; \pi/6]$ , without the need for other measurements, using

TABLE I  
COMPARISON BETWEEN ANALOG AND DIGITAL IMPLEMENTATIONS OF THE NEURON. THE REALIZATION TIME OF THE DIGITAL NN IS NOT MENTIONED SINCE THE NN STRUCTURE IS DIRECTLY IMPLEMENTED IN AN FPGA

	Analog implementation	Digital implementation
<b>Power consumption</b>	14mW	37.2mW
<b>Occupied area</b>	0.04mm <sup>2</sup>	104 slices / 204 LUT
<b>Resolution</b>	1mV	1mV
<b>Delay</b>	25ns	35ns
<b>Design time</b>	about 3 monthes	about 1 month
<b>Realisation time</b>	about 3 monthes	x
<b>Validation time</b>	about 1 month	about 1 month

multiple modulation frequencies of the laser diode or making the system structure more complex. For both applications, the same neural network was used, and electronic simulations and training phases were successfully performed with experimental measurements directly issued from the phase-shift laser range finder. Two types of neural network implementations have been realized. The analog implementation, integrated in a CMOS 0.35- $\mu\text{m}$  ASIC, allowed a lower power consumption than the one implemented in an FPGA. Nevertheless, the digital NN structure, developed in a shorter development time, had the advantage of being reconfigurable.

Moreover, the sensor will be more autonomous if the parameter update is achieved directly onboard the application as a function of the experimental conditions. On one hand, a fully digital NN structure has the advantage of limiting the number of ADC to be implemented, but will increase the processing time associated to the feedforward NN and simultaneously decrease the precision. On the other hand, a fully analog feedforward NN structure allows for a much lower power consumption for the MLP itself, yet the high number of necessary ADCs and DACs would also lead to a notable increase of the power consumption.

A solution that profits from both implementation method advantages might be the use of analog current multipliers and current adders, controlled by analog switches whose command will be digital [Fig. 9(c)]. Such a system might allow the use of only three ADCs—if the NN overall transfer equation is well determined with respect to each parameter—without any DAC. Furthermore, the power consumption and the signal processing time will be optimized. The analog switches can then also be used for controlling the NN architecture, by limiting or increasing the number of hidden neurons, for example, and then acquiring the ability of being structurally reconfigurable. Such a structure might be implemented in the optical head of the range finder, so that it allows the achievement of real-time distance range increase or surface discrimination directly onboard the system, whatever the variations of the experimental conditions are.

## REFERENCES

- [1] G. Hueber, T. Ostermann, T. Bauernfeind, R. Raschhofer, and R. Hagelauer, "New approach of ultrasonic distance measurement technique in robot applications," in *Proc. 5th Int. Conf. Signal Process.*, Aug. 21–25, 2000, vol. 3, pp. 2066–2069.
- [2] K. Zhang, C. Butler, Q. Yang, and Y. Lu, "A fiber optic sensor for the measurement of surface roughness and displacement using artificial neural networks," *IEEE Trans. Instrum. Meas.*, vol. 46, no. 4, pp. 899–902, Aug. 1997.
- [3] P. N. Pathirana and A. Zakhnich, "Surface identification by acoustic reflection characteristics using time delay spectrometry and artificial neural networks," in *Proc. IEEE Int. Conf. Neural Netw.*, Jun. 9–12, 1997, vol. 1, pp. 31–36.
- [4] M. J. Mendenhall and E. Merenyi, "Relevance-based feature extraction for hyperspectral images," *IEEE Trans. Neural Netw.*, vol. 19, no. 4, pp. 658–672, Apr. 2008.
- [5] V. Mitra, C.-J. Wang, and S. Banerjee, "Lidar detection of underwater objects using a neuro-SVM-based architecture," *IEEE Trans. Neural Netw.*, vol. 17, no. 3, pp. 717–731, May 2006.
- [6] L. I. Perlovsky and R. W. Deming, "Neural networks for improved tracking," *IEEE Trans. Neural Netw.*, vol. 18, no. 6, pp. 1854–1857, Nov. 2007.
- [7] D. G. Amorim, M. F. Delgado, and S. B. Ameneiro, "Polytope ARTMAP: Pattern classification without vigilance based on general geometry categories," *IEEE Trans. Neural Netw.*, vol. 18, no. 5, pp. 1306–1325, Sep. 2007.
- [8] S. L. Phung and A. Bouzerdoum, "A pyramidal neural network for visual pattern recognition," *IEEE Trans. Neural Netw.*, vol. 18, no. 2, pp. 329–343, Mar. 2007.
- [9] B. B. Nasution and A. I. Khan, "A hierarchical graph neuron scheme for real-time pattern recognition," *IEEE Trans. Neural Netw.*, vol. 19, no. 2, pp. 212–229, Feb. 2008.
- [10] S. Ozawa, S. Pang, and N. Kasabov, "Incremental learning of chunk data for online pattern classification systems," *IEEE Trans. Neural Netw.*, vol. 19, no. 6, pp. 1061–1074, Jun. 2008.
- [11] J. Tiecke, P. Schabel, and E. Rille, "Vehicle distance sensor using a segmented IR laser beam," in *Proc. 40th IEEE Veh. Technol. Conf.*, May 6–9, 1990, pp. 107–112.
- [12] Y. Omura, S. Funabiki, and T. Tanaka, "A monocular vision-based position sensor using neural networks for automated vehicle following," in *Proc. IEEE Int. Conf. Power Electron. Drive Syst.*, Jul. 27–29, 1999, vol. 1, pp. 388–393.
- [13] P. J. McKerrow and B. E. Kristiansen, "Classifying surface roughness with CTFM ultrasonic sensing," *IEEE Sensors J.*, vol. 6, no. 5, pp. 1267–1279, Oct. 2006.
- [14] M. K. Habib, "Fiber-grating-based vision system for real-time tracking, monitoring, and obstacle detection," *IEEE Sensors J.*, vol. 7, no. 1, pp. 105–121, Jan. 2007.
- [15] J. D. Williams, "Advanced technologies for perimeter intrusion detection sensors," in *Proc. Eur. Conv. Security Detection*, May 16–18, 1995, pp. 133–137.
- [16] F. Yang and M. Paindavoine, "Implementation of an RBF neural network on embedded systems: Real-time face tracking and identity verification," *IEEE Trans. Neural Netw.*, vol. 14, no. 5, pp. 1162–1175, Sep. 2003.
- [17] X. Miao, M. R. Azimi-Sadjadi, B. Tan, A. C. Dubey, and N. H. Witherspoon, "Detection of mines and minelike targets using principal component and neural-network methods," *IEEE Trans. Neural Netw.*, vol. 9, no. 3, pp. 454–463, May 1998.

- [18] H. Leung, G. Hennessey, and A. Drosopoulos, "Signal detection using the radial basis function coupled map lattice," *IEEE Trans. Neural Netw.*, vol. 11, no. 5, pp. 1133–1151, Sep. 2000.
- [19] P. Cinquin, E. Bainville, C. Barbe, E. Bittar, V. Bouchard, I. Bricault, G. Champleboux, M. Chenin, L. Chevalier, Y. Delnondedieu, L. Desbat, V. Dessenne, A. Hamadeh, D. Henry, N. Laieb, S. Lavallée, J. M. Lefebvre, F. Leitner, Y. Menguy, F. Padieu, O. Peria, A. Poyet, M. Promayon, S. Rouault, P. Sautot, J. Troccaz, and P. Vassal, "Computer assisted medical interventions," *IEEE Eng. Med. Biol. Mag.*, vol. 14, no. 3, pp. 254–263, May–Jun. 1995.
- [20] K. Maatta, J. Kostamoavaara, and R. Myllyla, "Profiling of hot surfaces by pulsed time-of-flight laser range finder techniques," *Appl. Opt.*, vol. 32, no. 27, pp. 5334–5347, Sep. 1993.
- [21] M. O'Farrell, E. Lewis, C. Flanagan, W. B. Lyons, and N. Jackman, "Design of a system that uses optical-fiber sensors and neural networks to control a large-scale industrial oven by monitoring the food quality online," *IEEE Sensors J.*, vol. 5, no. 6, pp. 1407–1420, Dec. 2005.
- [22] S. Yoda, H. Okabe, J. Takagi, and T. Yamashita, "Road surface recognition sensor using an optical spatial filter," in *Proc. Intell. Veh. Symp.*, Sep. 25–26, 1995, pp. 253–257.
- [23] J. Lan, T. Lan, and S. Nahavandi, "A novel application of a microaccelerometer for target classification," *IEEE Sensors J.*, vol. 4, no. 4, pp. 519–524, Aug. 2004.
- [24] S. K. Ozdemir, S. Shinohara, S. Ito, S. Takamiya, and H. Yoshida, "Compact optical instrument for surface classification using self-mixing interference in a laser diode," *Opt. Eng.*, vol. 40, no. 1, pp. 38–43, 2001.
- [25] P. Neelamegan and A. Rajendran, "Classification of surface roughness and distance measurement using artificial neural network," *Instrum. Sci. Technol.*, vol. 31, no. 4, pp. 417–423, 2003.
- [26] A. R. De Almeida, E. O. Freire, C. A. Ronnow, J. E. S. Vianna, and R. M. Rosi, "Neural network-based geometric references recognition applied to ultrasound echo signals," in *Proc. 43rd IEEE Midwest Symp. Circuits Syst.*, Aug. 8–11, 2000, vol. 3, pp. 1344–1347.
- [27] D. Castagnet, H. Tap-Béteille, and M. Lescure, "APD-based heterodyne optical head of a phase-shift laser rangefinder," *Opt. Eng.*, vol. 45, no. 4, pp. 43003\_1–43003\_7, Apr. 2006.
- [28] H. Tap-Béteille, D. Roviras, M. Lescure, A. Mallet, and F. Castanié, "Integration in CMOS technology of a high power amplifier predistorter," in *Proc. 8th Int. Workshop Signal Process. Space Commun.*, Catania, Italy, Sep. 24–26, 2003, pp. 24–26.
- [29] L. Gatet, H. Tap-Béteille, and M. Lescure, "Surface detection using phase-shift laser rangefinder and neural network," *Opt. Syst. Design*, vol. 46, no. 7, pp. 073002-1–073002-11, Jul. 2007.
- [30] L. Gatet, H. Tap-Béteille, and M. Lescure, "Analog neural network for real-time surface detection with a laser range finder," in *Proc. IEEE Instrum. Meas. Technol. Conf.*, May 1–3, 2007, pp. 1–6.
- [31] L. Gatet, H. Tap-Béteille, and M. Lescure, "Analog neural network implementation for a real-time surface classification application," *IEEE Sensors J.*, vol. 8, no. 8, pp. 1413–1421, Aug. 2008.
- [32] B. Journet, "Time of flight range finding systems," in *Proc. 7th Int. Symp. Laser Metrology Appl. Sci. Ind. Everyday Life*, 2002, vol. 4900, pp. 466–477.
- [33] T. Bosch and M. Lescure, "Experimental determination of the useful reflexion coefficient of non-cooperative targets for a time-of-flight laser range finder," *Opt. Rev.*, vol. 2, no. 4, pp. 289–291, 1995.
- [34] L. Gatet, H. Tap-Béteille, and M. Lescure, "Real time surface discrimination using an analog neural network implemented in a phase-shift laser range finder," *IEEE Sensors J.*, vol. 7, no. 10, pp. 1381–1387, Oct. 2007.



**Laurent Gatet** (S'06–M'08) was born in Paris, France, in 1980. He received the Ph.D. degree in microelectronics–microsystems from Electronics, Electrotechnology, Computer Science, Hydraulics, and Telecommunications Engineering School (ENSEEIHT), National Polytechnic Institute (INP), Toulouse University, Toulouse, France, in 2007.

Currently, he is with the French space agency, the National Center of Spatial Studies (CNES). His research interests are centered on neural network design and integration in the optoelectronic and spatial telecommunications fields.



**Hélène Tap-Béteille** (M'01) was born in 1973. She received the Ph.D. degree in microelectronics–microsystems from the Laboratoire d'Analyse et d'Architecture des Systèmes, French Centre National de la Recherche Scientifique (LAAS-CNRS), Toulouse, France, in 1999.

In 2001, she became an Assistant Professor with the Laboratory of Optoelectronics for Embedded Systems (LOSE), from Electronics, Electrotechnology, Computer Science, Hydraulics and Telecommunications Engineering School (ENSEEIHT), National Polytechnic Institute (INP), Toulouse University, Toulouse, France. She is currently working on integrated circuits and optoelectronics.



**Francis Bony** was born in 1975. He received the Ph.D. degree in microelectronics–microsystems from the Laboratoire d'Analyse et d'Architecture des Systèmes, French Centre National de la Recherche Scientifique (LAAS-CNRS), Toulouse, France, in 2003.

In 2005, he became an Assistant Professor with the Laboratory of Optoelectronics for Embedded Systems (LOSE), Electronics, Electrotechnology, Computer Science, Hydraulics and Telecommunications Engineering School (ENSEEIHT), National Polytechnic Institute (INP), Toulouse University, Toulouse, France. He is currently working on digital circuits and electronic system boards for optoelectronic measurement sensors.